ATOMIC-RESOLUTION ANALYSIS OF DEGRADATION PHENOMENA IN SOFCS: A Case Study of SO_2 Poisoning in LSM Cathodes

Takeshi Daio[1,2,3a], Pratoy Mitra[1a], Stephen M. Lyth[*4,5,6], and Kazunari Sasaki[1,2,3,4]

[1] Faculty of Engineering, Kyushu University
[2] International Research Center for Hydrogen Energy
[3] Next-Generation Fuel Cell Research Center (NEXT-FC)
[4] International Institute for Carbon-Neutral Energy Research (WPI-I2CNER), Kyushu University, Nishi-ku, Fukuoka, Japan
[5] School of Chemical and Process Engineering, University of Leeds, UK
[6] Department of Mechanical Engineering, University of Sheffield, UK
*Corresponding author: S.M.L (email: lyth@i2cner.kyushu-u.ac.jp).
[a]These authors contributed equally to this work.

Keywords: microscopy, SOFC, degradation, cathodes, sulfur, poisoning

<Corresponding author>
Stephen M. Lyth
International Institute for Carbon-Neutral Energy Research (I2CNER)
Kyushu University, Motooka 744, Nishi-ku,
Fukuoka 819-0395, JAPAN.
(Tel) +81-92-802-6742
(Fax) +81-92-802-6742
(email) lyth@i2cner.kyushu-u.ac.jp

Abstract

Solid oxide fuel cell (SOFC) degradation studies are often performed by scanning transmission electron microscopy (STEM), scanning electron microscopy (SEM), and X-ray diffraction (XRD). However, it is difficult to use these techniques to observe processes occurring at the smallest scales. Here, we study sulfur poisoning of $La_{0.8}Sr_{0.2}MnO_{3-\delta}$ (LSM) cathodes as a model case for atomic resolution scanning transmission electron microscopy (STEM) analysis with energy dispersive X-ray diffraction (EDX). Significant $SrSO_4$ nanoparticle formation is observed after SO_2 exposure, especially at grain boundaries in the LSM. In addition, La_2O_3 formation inside the grain was also confirmed. The formation of $SrSO_4$ is identified with irreversible SOFC degradation, in addition to simple SO_2 adsorption, which is reversible.

1. Introduction

Fuel cells are electrochemical energy conversion devices that can effectively convert the chemical energy of fuels directly into electricity via electrochemical reactions. Solid oxide fuel cells (SOFCs) operate at high temperature and therefore have faster reaction kinetics and can run on multiple different types of fuel.[1] However, the performance and durability of SOFCs can be seriously affected by impurities in the fuel feedstock, or in the oxidant supply (i.e. air). Impurities such as hydrogen sulphide (H_2S) in hydrocarbon fuels can cause serious degradation in performance at the anode. [2-4] H_2S and organosulfur compounds are commonly found in city gas, coal gas, and biogas. Sulfur levels of a few parts per million (ppm) are often added as odorants in city gas. These can degrade SOFC performance even at ppm levels. [13, 14] Sulfur also exists as contamination in the ambient air, mainly as sulfur dioxide (SO_2). Cathodic degradation due to this impurity is also possible, and has been studied for many different types of cathode material. [4-9,11-12] It is possible to purify air to remove sulfur, but this process is energy intensive and impractical at large scale. A detailed understanding of the poisoning mechanisms for specific impurities at both the anode and cathode is critical to achieve widespread SOFC commercialization. This has been studied in detail at the anode, but less so at the cathode. Here we focus on the latter.

Materials commonly used in SOFC cathodes are $La_{0.8}Sr_{0.2}MnO_{3-\delta}$ (LSM), or $La_{0.6}Sr_{0.4}Co_{0.2}Fe_{0.8}O_{3-\delta}$ (LSCF).[10] The role of LSM is as a pure electronic conductor, and this is mixed with scandia-stabilized zirconia (ScSZ) electrolyte. Scanning electron microscopy (SEM) and X-ray diffraction (XRD) have generally been employed to investigate poisoning mechanisms in such cathodes. [11, 12, 15] To date, two possible degradation initiation processes have been proposed. The first is that SO_2 adsorption leads to surface coverage, blocking the electrochemically active surface area. Sulfur can be relatively easily desorbed from the surface of LSM, and therefore this poisoning effect can be reversed. [14, 16] Indeed, performance recovery has been observed in LSM-based SOFCs after heating. [12] The second possible mechanism is that sulfur reacts with the cathode to form $SrSO_4$ precipitates, e.g. at grain boundaries.[17] SEM studies have highlighted areas where both Sr and S coexist, and XRD analysis has confirmed the signal of $SrSO_4$. [12] However, poisoning by $SrSO_4$ formation in LSM has not yet been fully confirmed at the microscopic level.

Although good progress has been made in understanding these systems using STEM, SEM and XRD, it is also extremely important to understand cathode degradation at

much higher spatial resolution. Changes in elemental composition within the grains are difficult to detect using these techniques. This is even more difficult in the initial stages of degradation. Therefore, investigations of LSM cathodes at the initial onset of degradation are still lacking. The early-stage sulfur poisoning processes are interesting to study at the nanoscale, as they may provide extra insight into the poisoning mechanism, rather than simply the end-state.

For the above reasons, we operated SOFCs with SO_2-containing air (40 ppm) supplied to the LSM cathodes, as an acceleration test. The resulting changes in composition and microstructure were investigated by atomic resolution STEM and EDX elemental mapping. The results are used to provide insight into the sulfur poisoning mechanism in SOFCs, especially in the early stages of operation.

2. Experimental

A typical electrolyte-supported cell was used for this work, with 200 μm thick ScSZ (10 mol% Sc_2O_3, 90 mol% ZrO_2) electrolyte plates. NiO-ScSZ cermet layers (56:44 mol% and 80:20 mol%) were screen printed on the anode side, followed by sintering in air at 1300˚C for 3 hours. LSM-ScSZ and then LSM were screen printed on

the cathode side, followed by sintering in air at 1200˚C for 5 hours. The geometric area of both electrodes was ca. 8 mm x 8 mm (0.64 cm^2). Pt meshes were attached to the electrode surfaces as current collectors. Pt paste with a geometric area of ca. 0.04 cm^2 was painted adjacent to the cathode as a reference electrode. The details of fabrication of this SOFC structure are reported in detail elsewhere,[18] and the conditions were chosen to simulate sulfur poisoning. The operation temperature was 750 °C, and ambient air was supplied to the cathode. 40 ppm of sulfur dioxide was introduced at 1 h for around 15 minutes. 3% humidified hydrogen was supplied to the anode. The open circuit voltage (OCV) was 1.05 V, the current was 128 mA (corresponding to a cuurent density of 200 mA/cm^2), and the cell was run for 25 hours. Gases were supplied at a temperature of 900 °C. A schematic image of the fuel cell configuration is shown in Fig. 1.

After sulfur poisoning tests, the cells were embedded in an epoxy resin by vacuum infiltration, in order to fill the pores. After cell operation, thinned samples were prepared for microscopic observation by focused-ion-beam (FIB, FB2100, Hitachi) milling, and mounted on copper grids. TEM-diffraction and STEM high-angle annular dark field (STEM-HAADF) images were acquired on a JEOL ARM-200F at 200 kV

with spherical aberration correction (CEOS, Germany). Elemental analysis was performed by energy dispersive X-ray spectrometry (EDX, Centurio, JEOL).

3. Results and discussion

Figure 1 shows the initial performance of the SOFC, degradation after SO_2 is introduced to the air supply, and partial recovery beginning at around 12.5 hours. This confirms the initial poisoning and subsequent recovery of performance observed in previous studies. [14, 16] Figure 2a shows an atomic resolution image of the surface of the LSM cathode after operation for 24 hours in the presence of SO_2. The area was selected from the surface of the LSM, facing a pore, and away from any grain boundaries (i.e. away from any precipitates, which are discussed later). The image is a top-down view of an atomic step with two terraces in the field of view. The step-height is estimated to be around 10 nm from the STEM focus depth. The variations in contrast are caused by electron scattering, and shifting of the focal plane. The crystal lattice of LSM is clearly visible. However some amorphous phase also seems to be present in the image, manifesting as patches of contrast change superimposed on the lattice. This is highlighted in a defocused image with increased contrast (Figure 2b). Figure 2c shows STEM-EDX

elemental mapping for sulfur in the same region. A strong signal is observed, confirming that sulfur is present in some form on the surface after SO_2 exposure. This sulfur content may be responsible for the amorphous phase observed in the original STEM image. Figure 2d shows the electron diffraction pattern for the same area of the sample. A strong pattern corresponding to crystalline LSM is observed, superimposed with a diffuse ring, corresponding to an amorphous phase. The above results are interpreted to confirm that amorphous phase of sulfur compound is present on the crystalline LSM surface after poisoning.

The same region is imaged at lower magnification in Figure 3, and EDX elemental mapping is performed for (a) strontium, (b) sulfur, and (c) oxygen. A composite image is shown in (d), whilst (e) and (f) show lanthanum and manganese maps, respectively. A stronger sulfur signal is detected at grain boundaries facing the pore void in this composite (showing up as black on the images). The sulfur is present at especially high concentration at the terrace edge, strongly suggesting that edge-adsorption partially drives the degradation process. In certain areas the concentration of strontium is higher in the region of high sulfur concentration, suggesting strontium diffusion towards adsorbed sulfur.

Figure 4 shows STEM-EDX images of the LSM at lower magnification, in which the grain boundaries are visible as linear black line across the sintered grains. In the STEM bright field image (Fig. 4a), the dark gray areas correspond to LSM grains, and the lighter areas correspond to pores filled with resin during FIB pre-processing. The dark linear features crossing the grain (highlighted by white arrows) are the LSM grain boundaries. Especially in (c) and (d), bright regions with high strontium and sulfur content are clearly observed, assumed to be $SrSO_4$. Many of these nanoscale features are observed preferentially at grain boundaries, as highlighted by black arrows in (a). This suggests that grain boundaries play an important role in nucleation of precipitates. [19] Additionally, sulfur is observed with lower concentration covering the whole area of the LSM.

A selected-area electron diffraction pattern of one of the sulfur-rich areas is shown in Figure 5a, showing high crystallinity. The inset shows the corresponding high-resolution STEM-HAADF image. Figure 5b shows a simulated electron diffraction pattern for $SrSO_4$, the structure of which is schematically represented in Figure 5c . [21] The crystal structure is orthorhombic, and the space group is Pnma. A strong correlation

between the observed and simulated diffraction patterns confirms that the sulfur-rich area observed on the LSM surface after SOFC operation is composed of $SrSO_4$. [20][21]

Figure 6a shows a cross-sectional STEM image of the interface between an LSM grain and a $SrSO_4$ nanoparticle. A grain boundary is clearly observed at the right hand side of the image, terminating at the edge of the $SrSO_4$ nanoparticle. Line profiles of the elemental distribution of Sr, La, Mn, and S were taken from the EDX map (Figure 6b). The S content is negligible within the LSM layer, but then increases sharply across the LSM/$SrSO_4$ interface and into the $SrSO_4$ material. This suggests that sulfur deposition is only at the surface, and negligible diffusion into the bulk occurs. The Sr concentration starts to decrease at around 100 nm before the interface, dropping by around 3 at% before sharply increasing in the $SrSO_4$ region. Conversely, the La concentration increases by around 3 at% within 100 nm of the interface. Electron diffraction patterns of the LSM near the interface, and of the bulk are shown in Figure 6c and 6d, respectively. Analysis of these images reveals that the lattice spacing expands by 0.5 % near the interface. This is in agreement with the increase in La content near the interface,

since La^{3+} has a larger Shannon ion diameter than Sr^{2+} (i.e. 0.115 nm compared with 0.113 nm). [22] This is discussed further in the next section.

Figure 7 shows cross-sectional STEM and EDX images of the LSM cathode with a prominent $SrSO_4$ nanoparticle on the surface. It is evident that the main part of the particle contains significant Sr, S, and O, but has very low La and Mn content. This is further an evidence that these particles are primarily formed as $SrSO_4$. However, another phase is also observed near the interface between LSM and $SrSO_4$. This third phase consists primarily of La (40 at%) and O (60 at%), corresponding well with the composition of La_2O_3. In the Sr, S and Mn maps this region is dark. This is also in agreement with the elemental line profiles taken in Figure 6, in which an increased La content near the interface was observed. Such La_2O_3 formation on the surface of LSM has been previously observed in humidity-dependent degradation studies. [23] In that case, La_2O_3 was formed across the surface by reaction between LSM and humidified air. Here, La_2O_3 is formed between LSM and $SrSO_4$. The formation of La_2O_3 in this case is assumed to result from a depletion of Sr in the LSM associated with formation of $SrSO_4$ at the surface. The lack of Mn observed in either the major or minor phases of this precipitate may be accounted for by enrichment of Mn in the LSM near the interface.

Alternatively, a pale feature is observed in the upper portion of the Mn, La and O maps, suggesting the formation of a third e.g. $LaMnO_3$ phase.

From the above experimental results, it is evident that significant $SrSO_4$ formation occurs on the LSM cathodes when SO_2 is present in significant amounts in air, even after just 24 hours of operation. Sulfur adsorption seems to occur preferentially at atomic steps and at grain boundaries, and is accompanied by the formation of La_2O_3, as Sr is depleted from the LSM. A possible mechanism for sulfur poisoning in LSM is illustrated in Figure 8. The first step is preferential SO_2 adsorption at an atomic step or grain boundary. The second step is reaction between SO_2 and LSM to form small amounts of $SrSO_4$. Sr ions are transported via bulk diffusion enabling the nucleation of $SrSO_4$ nanoparticles, especially along grain boundaries.[15] Within the single grains, Sr has a lower mobility, leading to local Sr depletion and thus resulting in the La_2O_3 formation.

It has been previously shown that if adsorbed SO_2 forms sulfite and sulfate species, the poisoning effect is irreversible. [16] If the SO_2 is simply adsorbed on the surface it can be easily desorbed and the SOFC performance can be recovered.[14] Here we have

shown that significant $SrSO_4$ formation does occur at grain boundaries and therefore that full recovery of SOFC performance after the SO_2 poisoning would be unlikely. However, the sulfur distribution observed across the whole LSM surface suggests that both processes may occur to a certain extent, explaining a partial recovery of cell performance in previous studies.

4. Conclusion

Early-stage sulfur poisoning of LSM cathodes in SOFCs was investigated by atomic resolution STEM. Strong sulfur signals were observed on the LSM surface after SO_2 exposure, especially at atomic edges and grain boundaries. The growth of $SrSO_4$ nanoparticles on the surface at grain boundaries was confirmed, accompanied with Sr depletion and La_2O_3 formation in the LSM. The preferential formation of $SrSO_4$ at grain boundaries is attributed to faster Sr ion transport at grain boundaries compared with the bulk. This study confirms that $SrSO_4$ formation is probably the dominant mechanism for the performance degradation in LSM-based SOFCs exposed to SO_2, even in the early stages of operations, and therefore that it is largely irreversible. This study is an

example of how atomic resolution microscopy can contribute to fuel cell poisoning studies.

Acknowledgments

This research is supported by the Japan Science and Technology Agency (JST) through its “Center of Innovation“ Science and Technology based Radical Innovation and Entrepreneurship Program (COI Program) to establish advanced analytical methods for fuel cells. The International Institute for Carbon-Neutral Energy Research is supported by World Premier International Research Center Initiative (WPI), MEXT, Japan.

References

[1] Stambouli AB, Traversa E. Solid oxide fuel cells (SOFCs): a review of an environmentally clean and efficient source of energy. Renewable and Sustainable Energy Reviews. 2002;6:433-55.

[2] Haga K, Adachi S, Shiratori Y, Itoh K, Sasaki K. Poisoning of SOFC anodes by various fuel impurities. Solid State Ionics. 2008;179:1427-31.

[3] Sasaki K, Susuki K, Iyoshi A, Uchimura M, Imamura N, Kusaba H, et al. H_2S poisoning of solid oxide fuel cells. Journal of the Electrochemical Society. 2006;153:A2023-A9.

[4] Sasaki K, Haga K, Yoshizumi T, Minematsu D, Yuki E, Liu R, et al. Chemical durability of Solid Oxide Fuel Cells: Influence of impurities on long-term performance. Journal of power Sources. 2011;196:9130-40.

[5] Yang L, Wang S, Blinn K, Liu M, Liu Z, Cheng Z, et al. Enhanced sulfur and coking tolerance of a mixed ion conductor for SOFCs: $BaZr_{0.1}Ce_{0.7}Y_{0.2-x}YbxO_{3-\delta}$. Science. 2009;326:126-9.

[6] Schuler AJ, Wuillemin Z, Hessler-Wyser A, Van Herle J. Sulfur as pollutant species on the cathode side of a SOFC system. ECS Transactions. 2009;25:2845-52.

[7] Schuler JA, Gehrig C, Wuillemin Z, Schuler AJ, Wochele J, Ludwig C, et al. Air side contamination in solid oxide fuel cell stack testing. Journal of Power Sources. 2011;196:7225-31.

[8] Schuler JA, Yokokawa H, Calderone CF, Jeangros Q, Wuillemin Z, Hessler-Wyser A. Combined Cr and S poisoning in solid oxide fuel cell cathodes. Journal of Power Sources. 2012;201:112-20.

[9] De-jun W, Jing L. Effect of SO_2 on Performance of Solid Oxide Fuel Cell Cathodes. CHEMICAL RESEARCH IN CHINESE UNIVERSITES. 2012;28:866-8.

[11] Wang F, Yamaji K, Cho D-H, Shimonosono T, Kishimoto H, Brito ME, et al. Effect of strontium concentration on sulfur poisoning of LSCF cathodes. Solid State Ionics. 2012;225:157-60.

[12] Xiong Y, Yamaji K, Horita T, Yokokawa H, Akikusa J, Eto H, et al. Sulfur poisoning of SOFC cathodes. Journal of The Electrochemical Society. 2009;156:B588-B92.

[13] Yang L, Wang S, Blinn K, Liu M, Liu Z, Cheng Z, et al. Enhanced sulfur and coking tolerance of a mixed ion conductor for SOFCs: $BaZr_{0.1}Ce_{0.7}Y_{0.2-x}YbxO_{3-\delta}$. Science. 2009;326:126-9.

[14] Wang F, Yamaji K, Cho D-H, Shimonosono T, Kishimoto H, Brito ME, et al. Sulfur Poisoning on $La_{0.6}Sr_{0.4}Co_{0.2}Fe_{0.8}O_3$ Cathode for SOFCs. Journal of The Electrochemical Society. 2011;158:B1391-B7.

[15] Wang CC, Chen K, Jiang SP. Sulfur Deposition and Poisoning of $La_{0.6}Sr_{0.4}Co_{0.2}Fe_{0.8}O_{3-\delta}$ Cathode Materials of Solid Oxide Fuel Cells. Journal of The Electrochemical Society. 2014;161:F1133-F9.

[16] Schuler AJ, Wuillemin Z, Hessler-Wyser A, Van Herle J. Sulfur as pollutant species on the cathode side of a SOFC system. ECS Transactions. 2009;25:2845-52.

[17] Bucher E, Gspan C, Hofer F, Sitte W. Sulphur poisoning of the SOFC cathode material $La_{0.6}Sr_{0.4}CoO_{3-\delta}$. Solid State Ionics. 2013;238:15-23.

[18] Kim SH, Ohshima T, Shiratori Y, Itoh K, Sasaki K. Effect of Water Vapor and SOx in Air on the Cathodes of Solid Oxide Fuel Cells. MRS Proceedings: Cambridge Univ Press; 2007. p. 1041-R03-10.

[19] Horita T, Sakai N, Kawada T, Yokokawa H, Dokiya M. Grain‐Boundary Diffusion of Strontium in (La, Ca) CrO_3 Perovskite‐Type Oxide by SIMS. Journal of the American Ceramic Society. 1998;81:315-20.

[20] Wong-Ng W, McMurdie H, Hubbard C, Mighell A. JCPDS-ICDD research associateship (cooperative program with NBS/NIST). JOURNAL OF RESEARCH-NATIONAL INSTITUTE OF STANDARDS AND TECHNOLOGY. 2001;106:1013-28."

[21] Garske D, Peacor DR. Refinement of the structure of celestite SrSO4. Zeitschrift für Kristallographie-Crystalline Materials. 1965;121:204-10.

[22] Shannon Rt. Revised effective ionic radii and systematic studies of interatomic distances in halides and chalcogenides. Acta Crystallographica Section A: Crystal Physics, Diffraction, Theoretical and General Crystallography. 1976;32:751-67.

[23] Liu R, Kim S, Taniguchi S, Oshima T, Shiratori Y, Ito K, et al. Influence of water vapor on long-term performance and accelerated degradation of solid oxide fuel cell cathodes. Journal of power Sources. 2011;196:7090-6.

Figure captions

Figure 1. (a) Schematic of the fuel cell set-up used in this study. (b) Short term electrochemical durability test in the presence of SO_2, indicating a slight recovery in performance after around 12.5 hours.

Figure 2. (a) STEM-HAADF image of the surface of a sulfur-poisoned LSM cathode, away from any grain boundaries. (b) Defocussed image of the same area, highlighting an amorphous phase. (c) EDX elemental mapping of sulfur in the same area. The dashed line shows the position of the atomic step. (d) Electron diffraction pattern showing the characteristic refection of crystalline LSM superimposed with a broader amorphous phase.

Figure 3. STEM-EDX elemental mapping of the LSM cathode after the SO_2 exposure: (a) strontium, (b) sulfur, (c) oxygen, and (d) composite image (green = Sr, red = S, blue = O). (e) and (f) shows lanthanum and manganese.

Figure 4. (a) Low-magnification STEM-bright field image of the LSM cathode after the SO_2 poisoning. STEM-EDX mapping of (b) La, (c) Sr, and (d) S. Sulfur- and

strontium-rich features are preferentially observed at grain boundaries (indicated by arrows).

Figure 5. (a) STEM-HAADF atomic resolution image of an S- and Sr-rich precipitate as observed in Figure 3. (b) Electron diffraction pattern of the same area. (c) Simulated electron diffraction pattern for $SrSO_4$. (d) Atomic arrangement corresponding to the simulated $SrSO_4$ diffraction pattern.

Figure 6. (a) STEM image of the interface between LSM and $SrSO_4$. (b) EDX line profiles across the interface. (c) Electron diffraction patterns of LSM near the interface, and (d) within the bulk.

Figure 7. (a) STEM-HAADF image and (b-f) EDX maps of the LSM cathode after the SO_2 exposure. Schematic representations of (g) SO_2 adsorption and enrichment in, and (h) precipitate formation and Sr depletion in LSM.

Figure 8. Schematic representation of the degradation mechanism of LSM cathodes in the presence of SO_2.

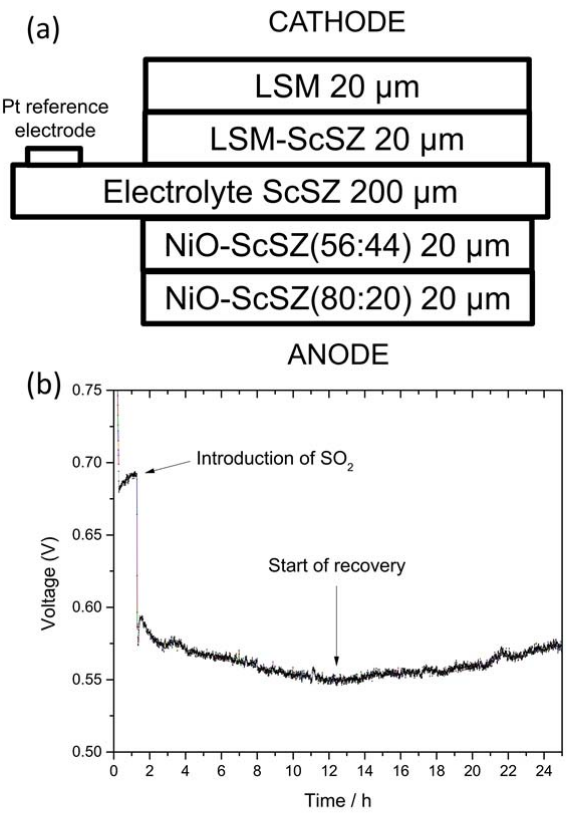

Figure 1. (a) Schematic of the fuel cell set-up used in this study. (b) Short term electrochemical durability test in the presence of SO_2, indicating a slight recovery in performance after around 12.5 hours.

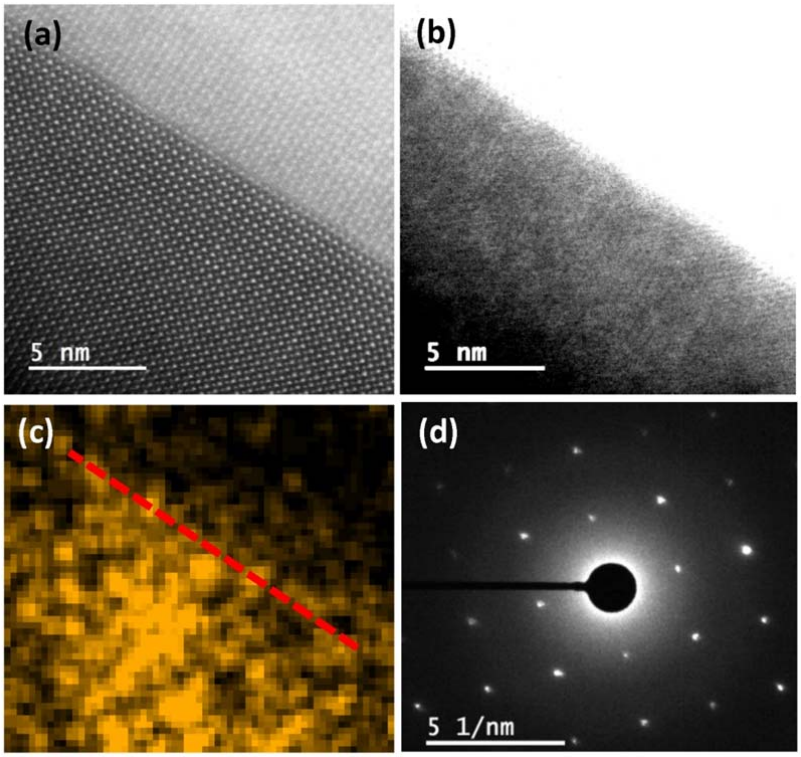

Figure 2. (a) STEM-HAADF image of the surface of a sulfur-poisoned LSM cathode, away from any grain boundaries. (b) Defocussed image of the same area, highlighting an amorphous phase. (c) EDX elemental mapping of sulfur in the same area. The dashed line shows the position of the atomic step. (d) Electron diffraction pattern showing the characteristic refection of crystalline LSM superimposed with a broader amorphous phase.

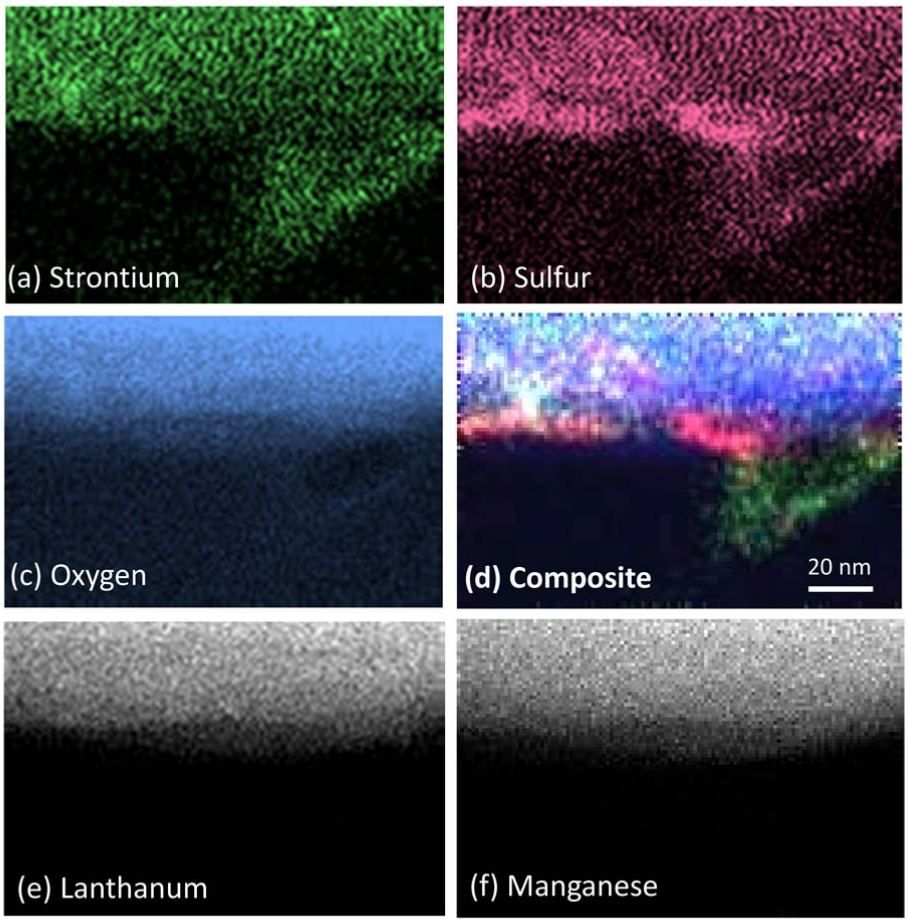

Figure 3. STEM-EDX elemental mapping of an LSM cathode after SO_2 exposure: (a) strontium, (b) sulfur, (c) oxygen, and (d) composite image (green = Sr, red = S, blue = O). (e) and (f) show lanthanum and manganese maps.

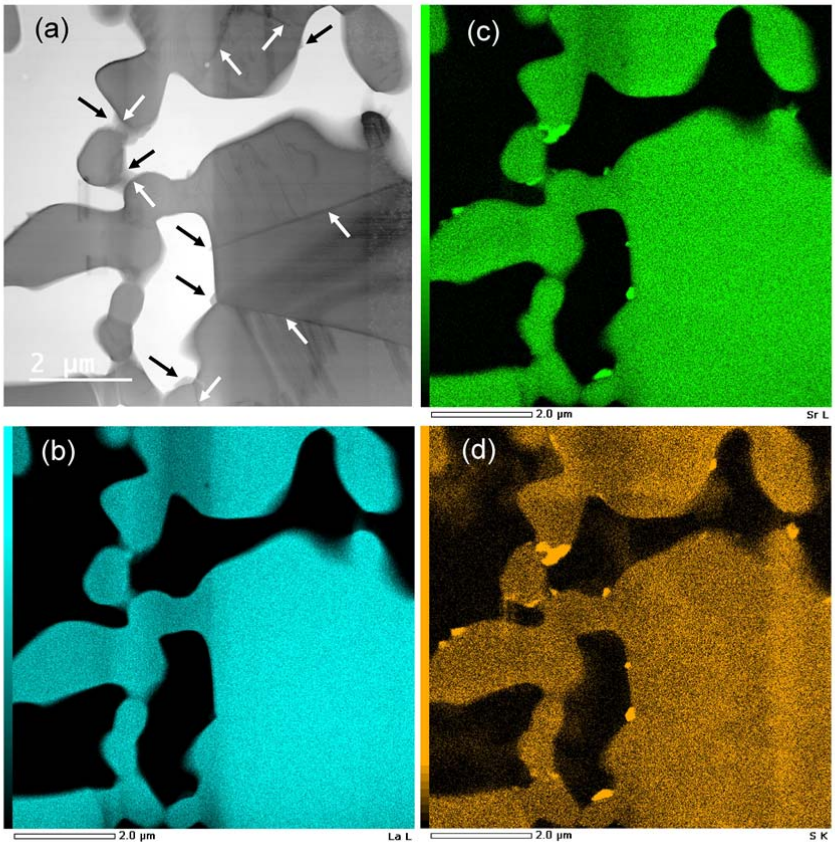

Figure 4. (a) Low-magnification STEM-bright field image of the LSM cathode after the SO_2 poisoning. STEM-EDX mapping of (b) La, (c) Sr, and (d) S. Sulfur- and strontium-rich precipitates are preferentially observed at grain boundaries (indicated by arrows).

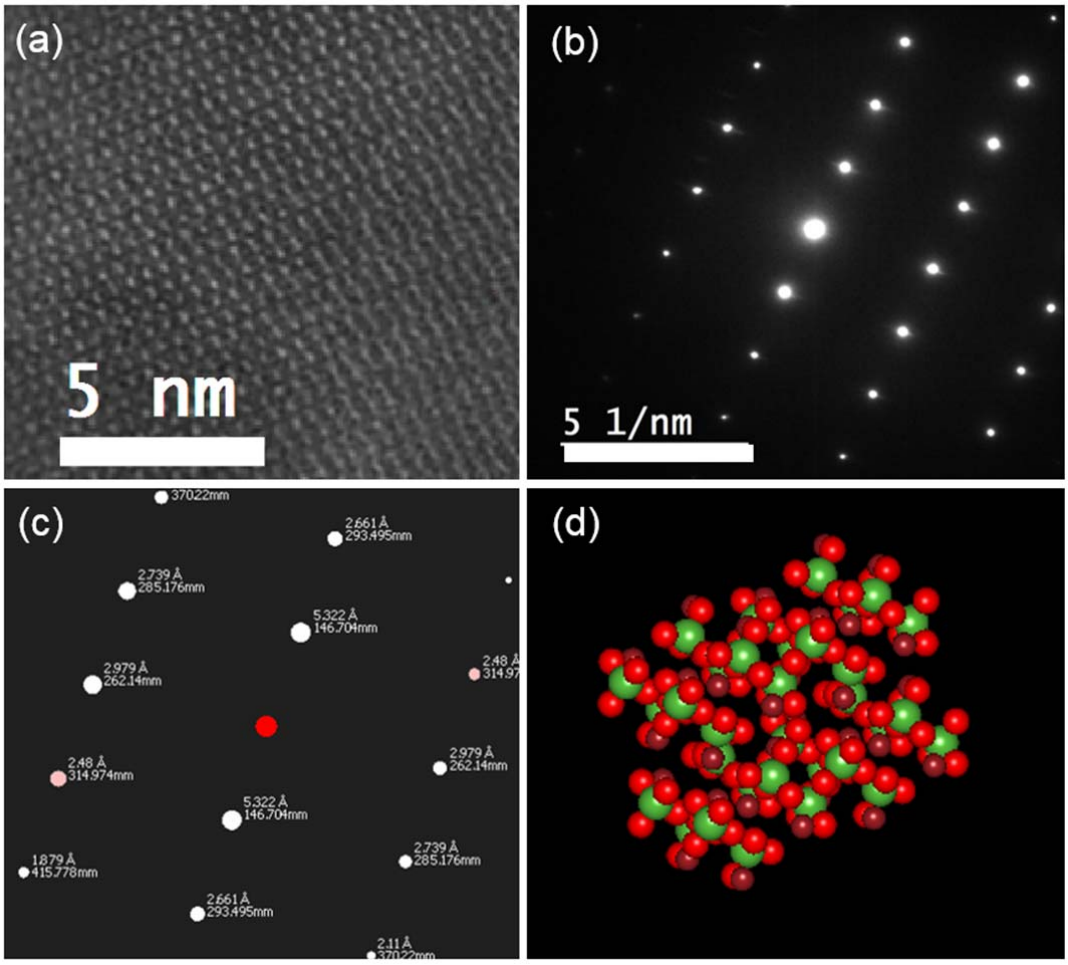

Figure 5. (a) STEM-HAADF atomic resolution image of an S- and Sr-rich precipitate as observed in Figure 3. (b) Electron diffraction pattern of the same area. (c) Simulated electron diffraction pattern for $SrSO_4$. (d) Atomic arrangement corresponding to the simulated $SrSO_4$ diffraction pattern.

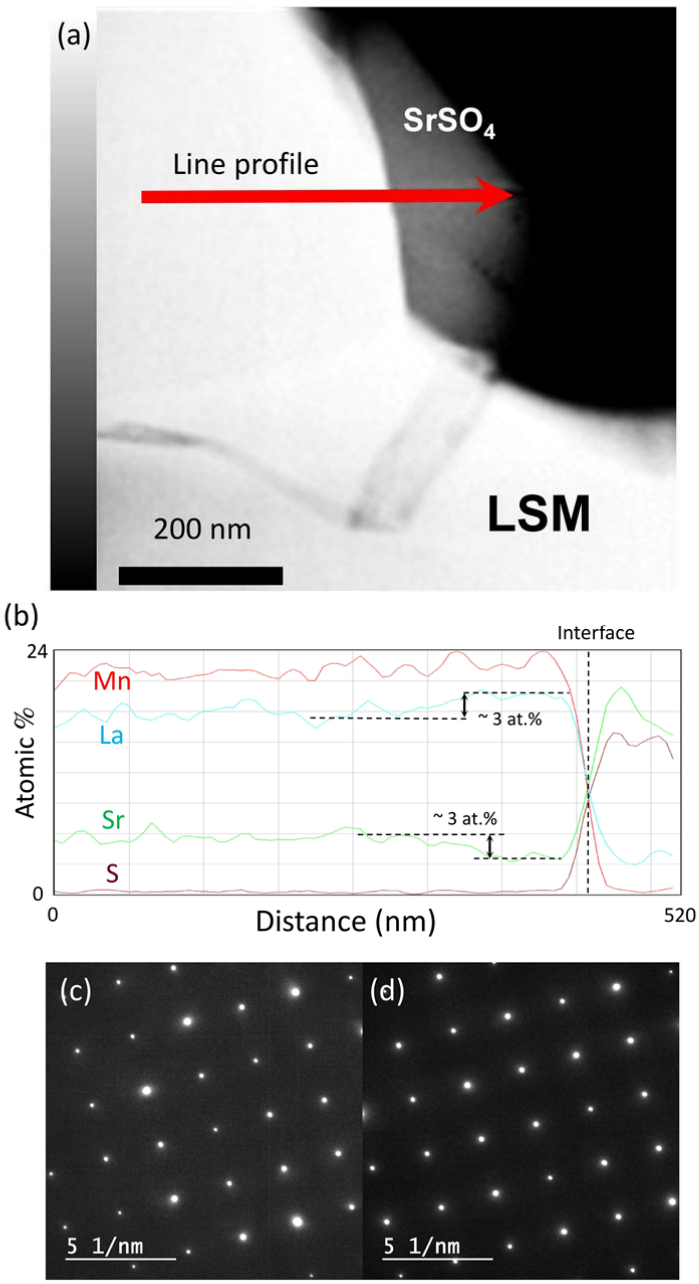

Figure 6. (a) STEM image of the interface between LSM and $SrSO_4$. (b) EDX line profiles across the interface. (c) Electron diffraction patterns of LSM near the interface, and (d) within the bulk.

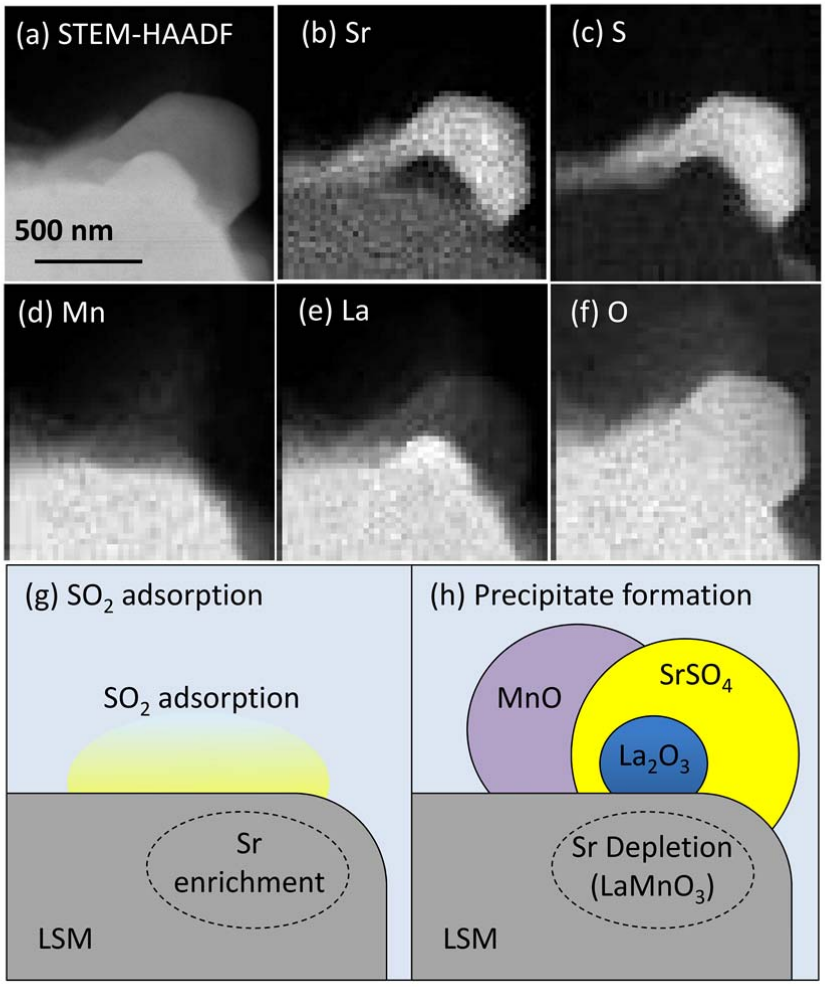

Figure 7. (a) STEM-HAADF image and (b-f) EDX maps of the LSM cathode after the SO_2 exposure. Schematic representations of (g) SO_2 adsorption and enrichment in, and (h) precipitate formation and Sr depletion in LSM.

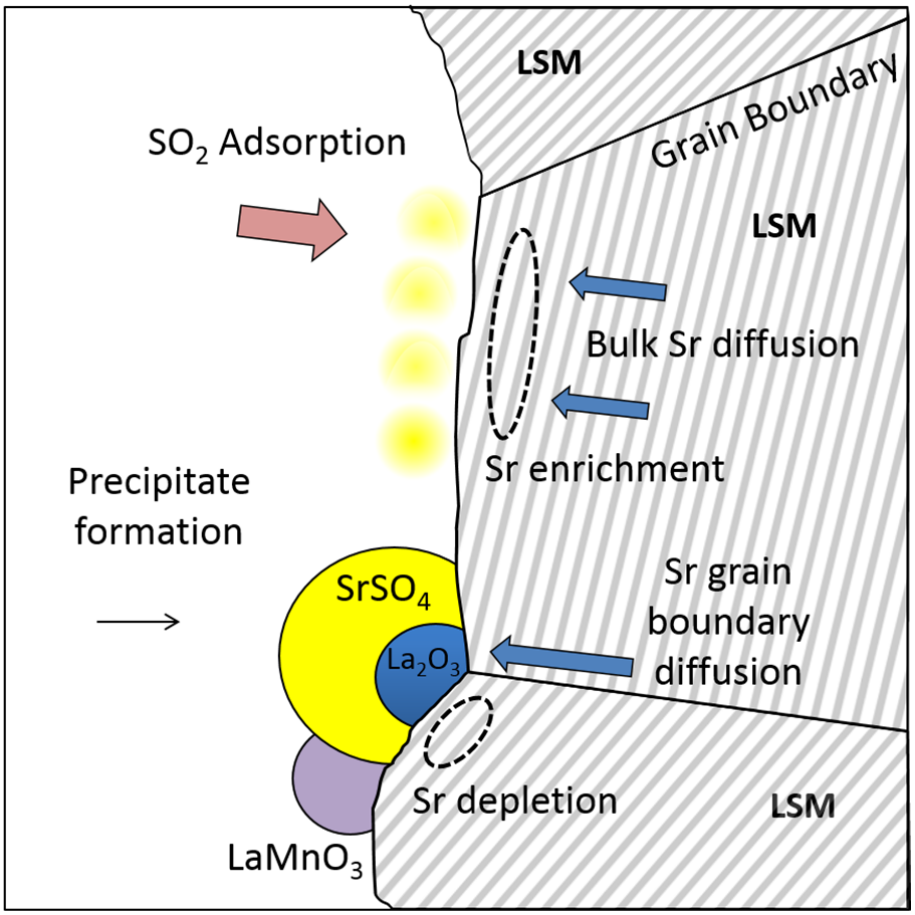

Figure 8. Schematic representation of the degradation mechanism of LSM cathodes in the presence of SO_2.